

Robust Production of 2D Quantum Sheets from Bulk Layered Materials

[Supplementary information]

Yuanqing Xu^{1,2}, Shulin Chen^{3,4}, Zhipeng Dou^{3,5}, Yanhong Ma¹, Yang Mi⁶, Wenna Du⁶,
Yin Liu⁷, Jianqi Zhang¹, Jinqian Chang¹, Cheng Liang¹, Jin Zhou¹, Hongbo Guo⁸,
Peng Gao^{3,9,10}, Xinfeng Liu⁶, Yanke Che⁷ and Yong Zhang^{1,2*}

¹CAS Key Laboratory of Nanosystem and Hierarchical Fabrication, CAS Center for Excellence in Nanoscience, National Center for Nanoscience and Technology, Beijing 100190, P. R. China.

²University of Chinese Academy of Sciences, Beijing 100049, P. R. China.

³Electron Microscopy Laboratory, School of Physics, Peking University, Beijing 100871, P. R. China.

⁴State Key Laboratory of Advanced Welding and Joining, Harbin Institute of Technology, Harbin 150001, P. R. China.

⁵Key Laboratory for Micro-/Nano-Optoelectronic Devices of Ministry of Education, School of Physics and Electronics, Hunan University, Changsha 410082, P. R. China.

⁶CAS Key Laboratory of Standardization and Measurement for Nanotechnology, CAS Center for Excellence in Nanoscience, National Center for Nanoscience and Technology, Beijing 100190, P. R. China.

⁷CAS Key Laboratory of Photochemistry, CAS Research/Education Center for Excellence in Molecular Sciences, Institute of Chemistry, Chinese Academy of Sciences, Beijing 100190, P. R. China.

⁸CAS Key Laboratory for Biomedical Effects of Nanomaterials and Nanosafety, CAS Center for Excellence in Nanoscience, National Center for Nanoscience and Technology, Beijing 100190, P. R. China.

⁹Collaborative Innovation Center of Quantum Matter, Beijing 100871, P. R. China.

¹⁰International Center for Quantum Materials, School of Physics, Peking University, Beijing 100871, P. R. China.

*e-mail: zhangyong@nanoctr.cn

This PDF file includes:

- ◆ **Fig. S1. SEM images of the bulk layered materials.**
- ◆ **Fig. S2. SEM images of silica microspheres during ball-milling.**
- ◆ **Fig. S3. SEM images of graphite during silica-assisted ball-milling.**
- ◆ **Fig. S4. Schematic illustration of the redispersion process.**
- ◆ **Fig. S5. Solvent diversity and solvability towards redispersion of GQs, BNQs, and MoS₂ Qs.**
- ◆ **Fig. S6. Zeta potential of the QS aqueous dispersions.**
- ◆ **Fig. S7. TEM image and lateral size distribution of WS₂ Qs.**
- ◆ **Fig. S8. AFM image and height distribution of WS₂ Qs.**
- ◆ **Fig. S9. UV-vis absorption spectra of WS₂ Qs.**
- ◆ **Fig. S10. Raman spectra of WS₂ Qs.**
- ◆ **Fig. S11. XRD patterns of WS₂ Qs.**
- ◆ **Fig. S12. XPS spectra of GQs, BNQs, and MoS₂ Qs.**
- ◆ **Fig. S13. PL spectra of WS₂ Qs/NMP dispersions at varying excitation wavelengths.**
- ◆ **Fig. S14. PL spectra of the QS dispersions.**
- ◆ **Fig. S15. Quantum yields of BNQs in varying solvents.**
- ◆ **Fig. S16. TEM image of (BNQs-PMMA) cross-section and corresponding SAXS image.**
- ◆ **Fig. S17. TEM image of (MoS₂ Qs-PMMA) cross-section and corresponding SAXS image.**
- ◆ **Fig. S18. PL spectra of Qs-PMMA thin films at the excitation wavelength of 360 nm.**

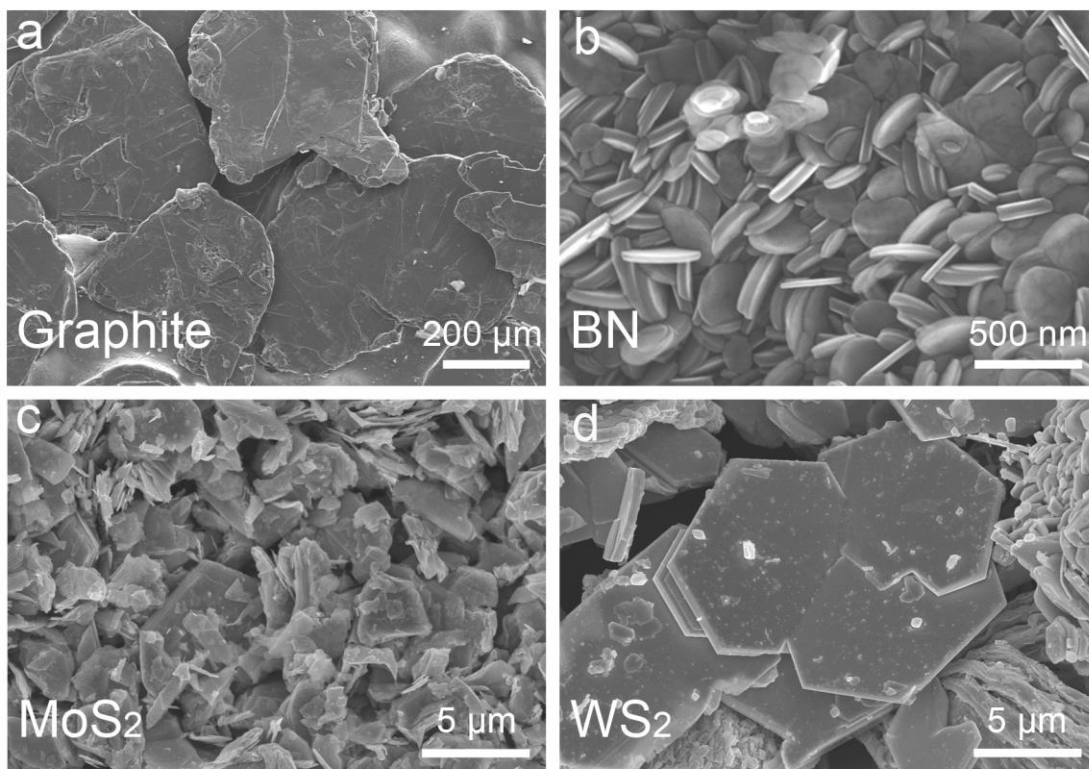


Fig. S1. SEM images of the bulk layered materials. Graphite (a), BN (b), MoS₂ (c), and WS₂ (d).

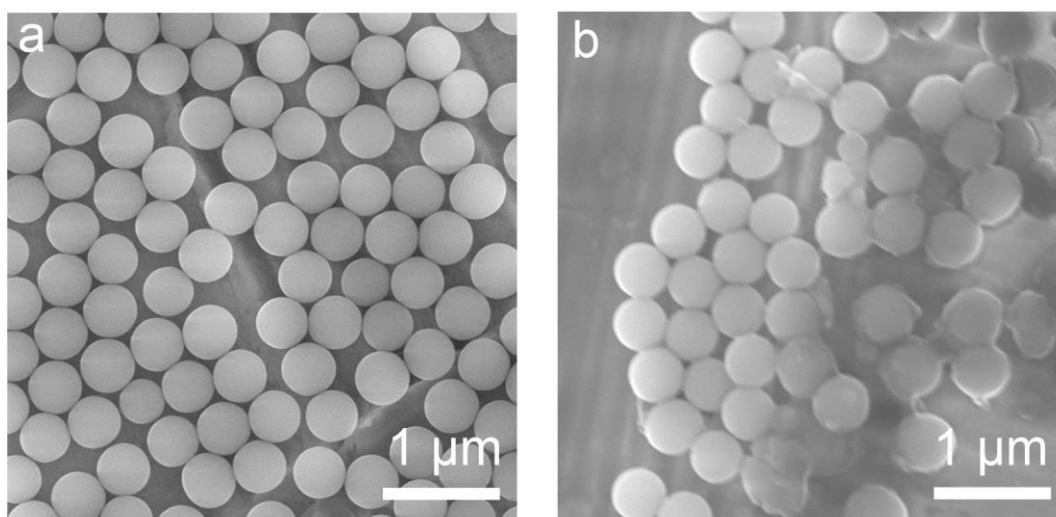


Fig. S2. SEM images of silica microspheres during ball-milling. (a) Before ball-milling, (b) After ball-milling for 12h (agate balls: silica microspheres: graphite = 100: 10: 1 by weight).

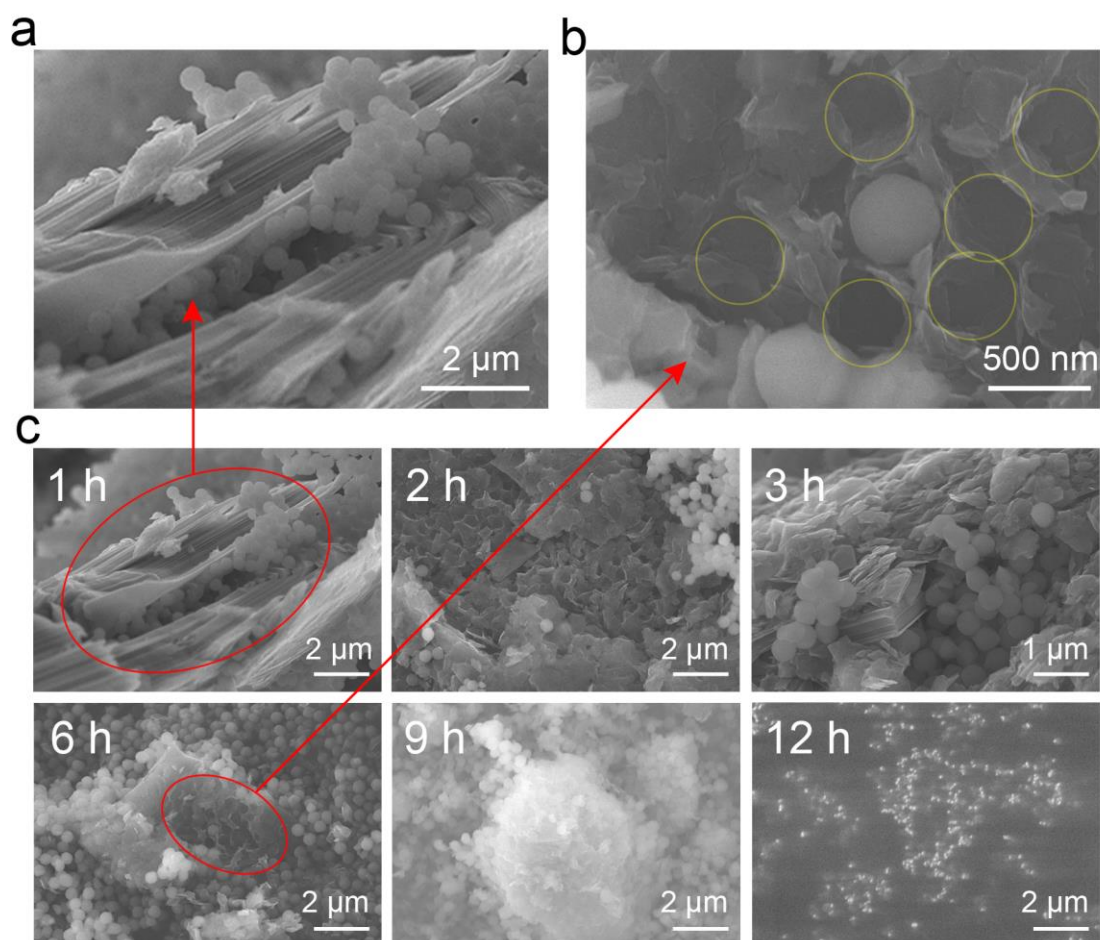


Fig. S3. SEM images of graphite during silica-assisted ball-milling. (a) Graphite interlayers inserted by silica microspheres. (b) Graphite surfaces severely cracked and well blended with silica microspheres and their voids. (c) Evolution of graphite with increasing ball-milling time.

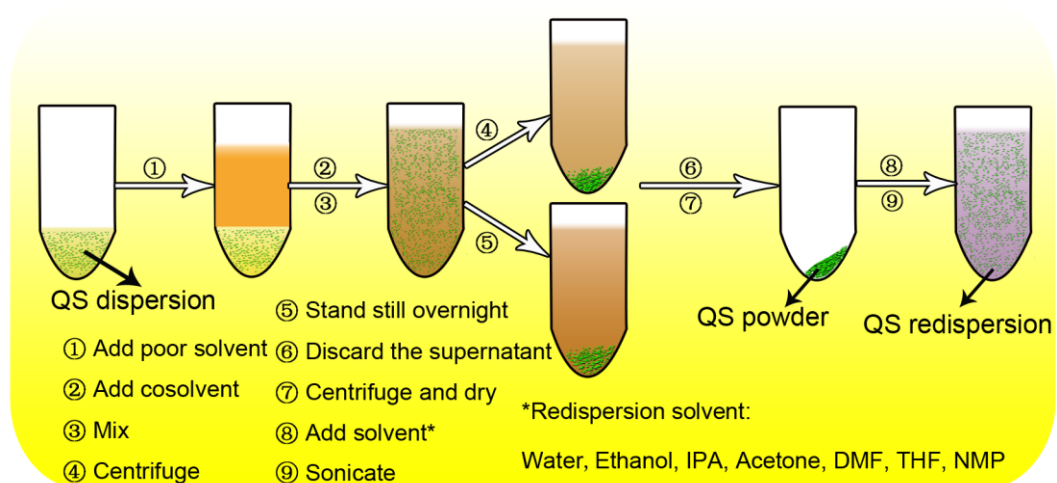


Fig. S4. Schematic illustration of the redispersion process.

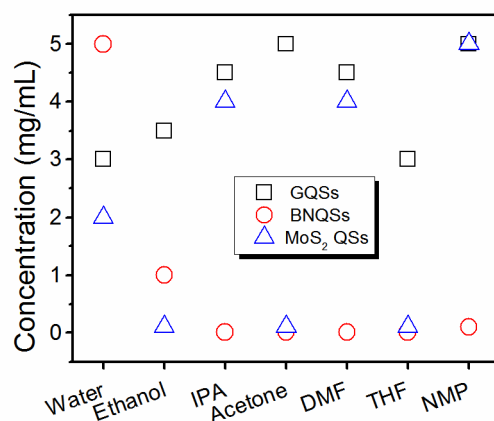


Fig. S5. Solvent diversity and solvability towards redispersion of GQs, BNQs, and MoS₂ Qs.

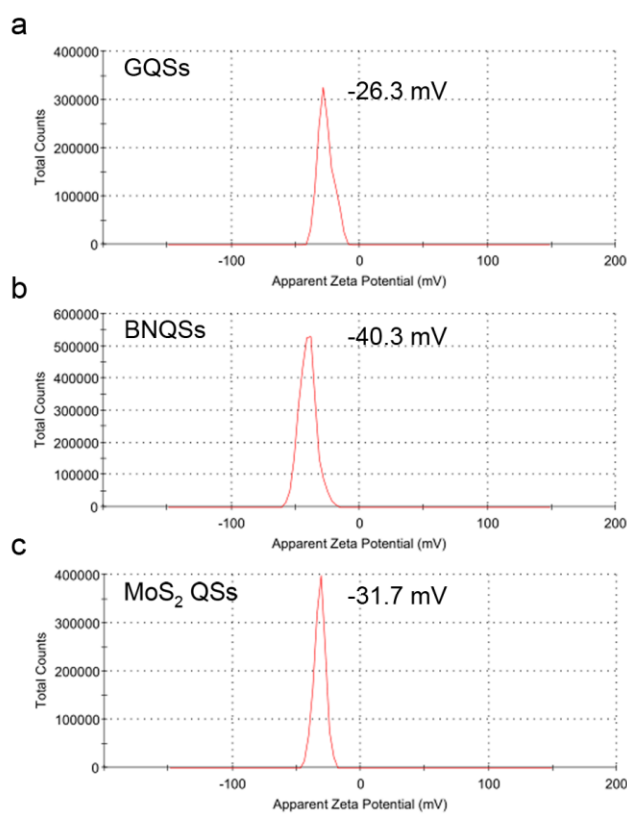


Fig. S6. Zeta potential of the QS aqueous dispersions. GQs (a), BNQs (b), and MoS₂ Qs (c). The concentration for each dispersion is 0.1 mg/mL.

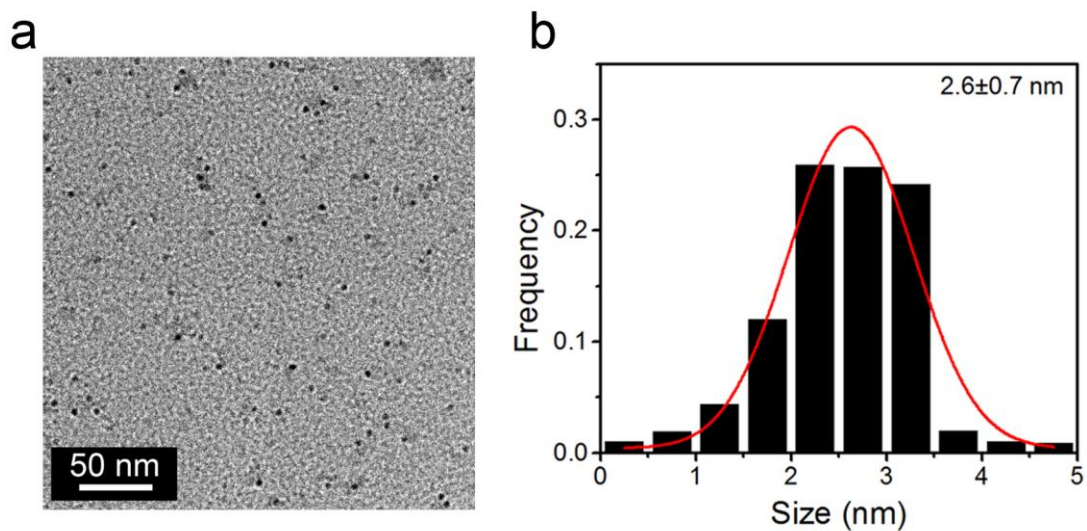


Fig. S7. TEM image (a) and lateral size distribution (b) of WS₂ QDs.

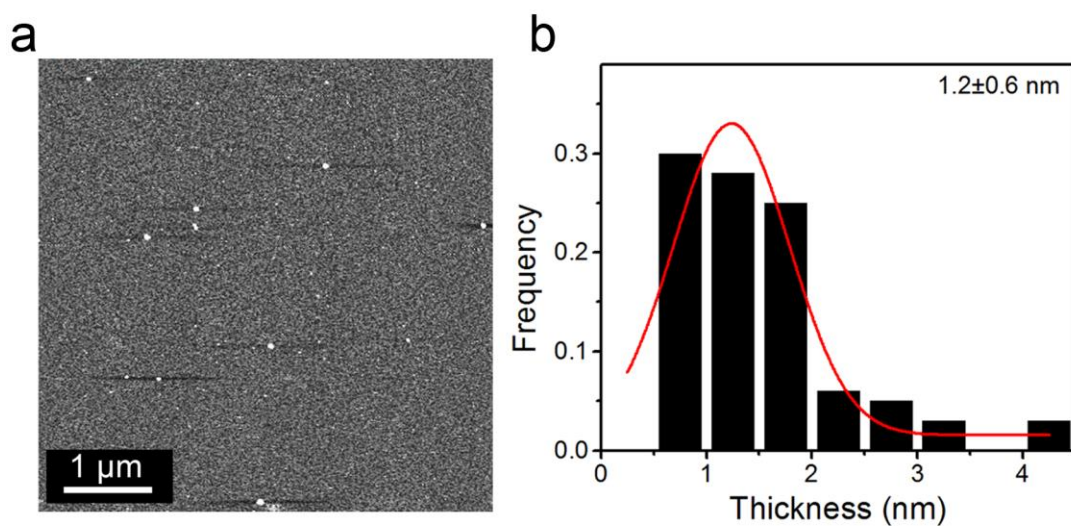


Fig. S8. AFM image (a) and height distribution (b) of WS₂ QDs.

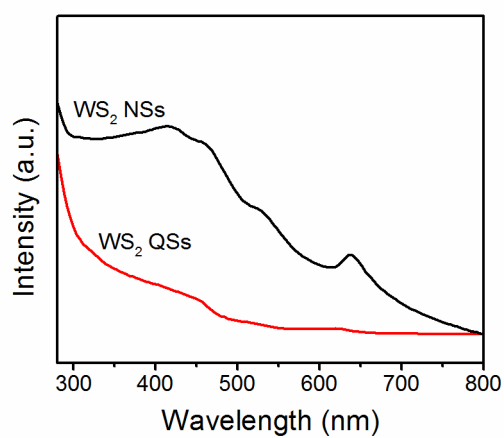


Fig. S9. UV-vis absorption spectra of WS₂ QSs. Data for WS₂ NSs are shown for comparison.

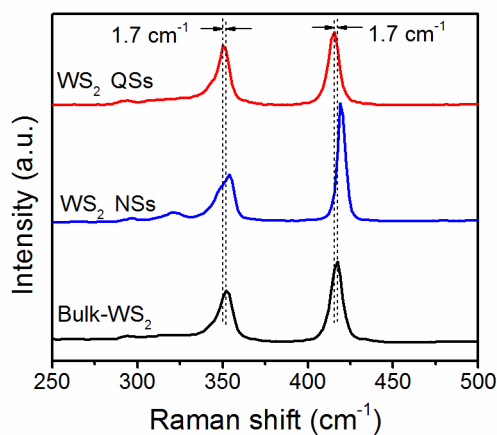


Fig. S10. Raman spectra of WS₂ QSs. Data for WS₂ NSs and bulk materials are shown for comparison.

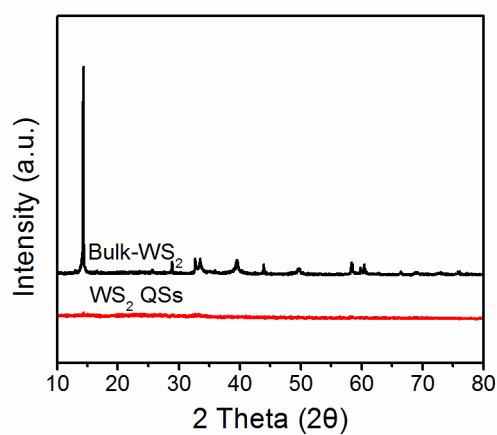


Fig. S11. XRD patterns of WS₂ QSs. Data for bulk materials are shown for comparison.

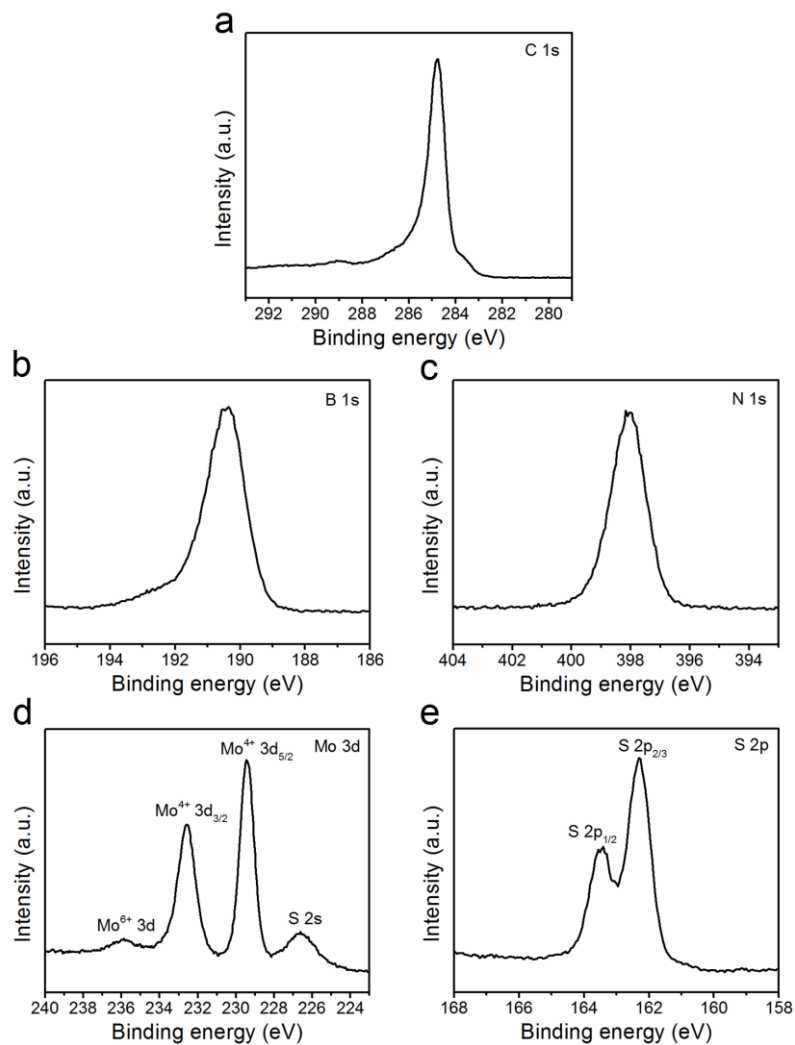


Fig. S12. XPS spectra of GQs (a), BNQs (b, c), and MoS₂ Qs (d, e).

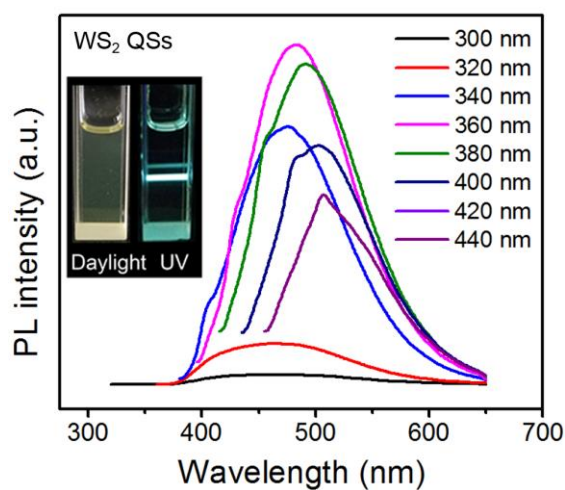


Fig. S13. PL spectra of WS₂ Qs/NMP dispersions at varying excitation wavelengths.

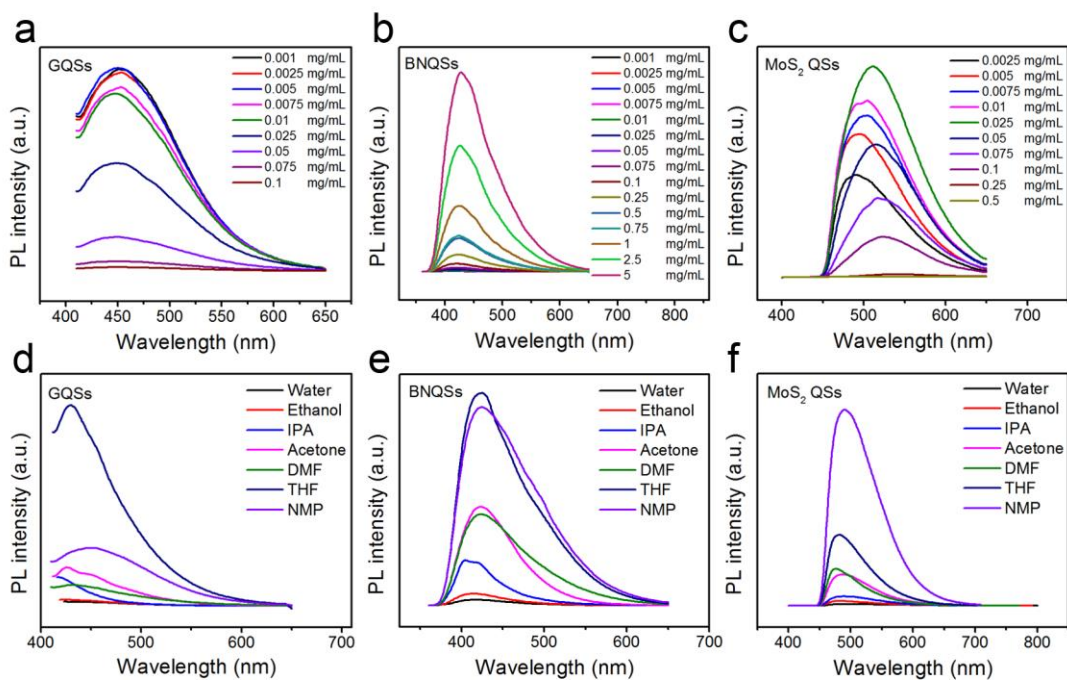


Fig. S14. PL spectra of the QS dispersions. (a-c) With varying concentrations. The solvent is NMP, H₂O, NMP respectively. (d-f) In varying solvents. The concentration is fixed at 0.01 mg/mL. The excitation wavelength for the GQS (a,d), BNQS (b,e), and MoS₂ QS (c,f) dispersions is 360 nm, 330 nm, and 380 nm respectively.

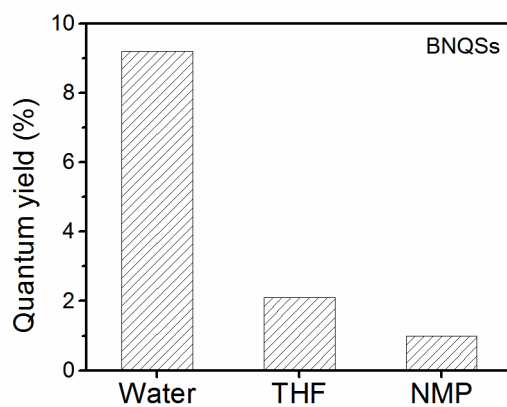


Fig. S15. Quantum yields of BNQSs in varying solvents. The excitation wavelength is 330 nm. The concentration is fixed at 0.01 mg/mL.

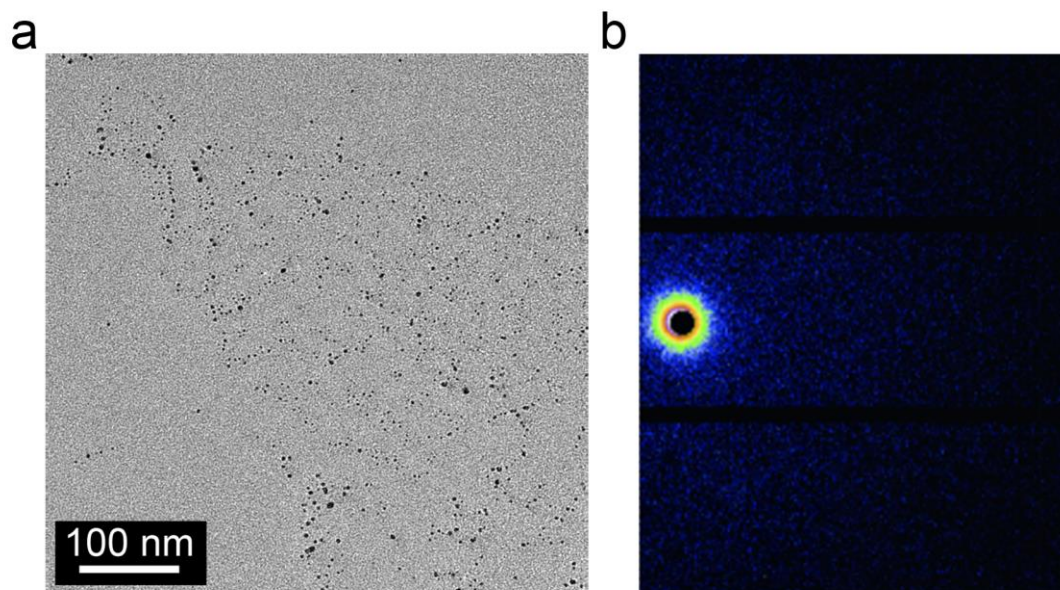


Fig. S16. TEM image of (BNQs-PMMA) cross-section (a) and corresponding SAXS image (b).

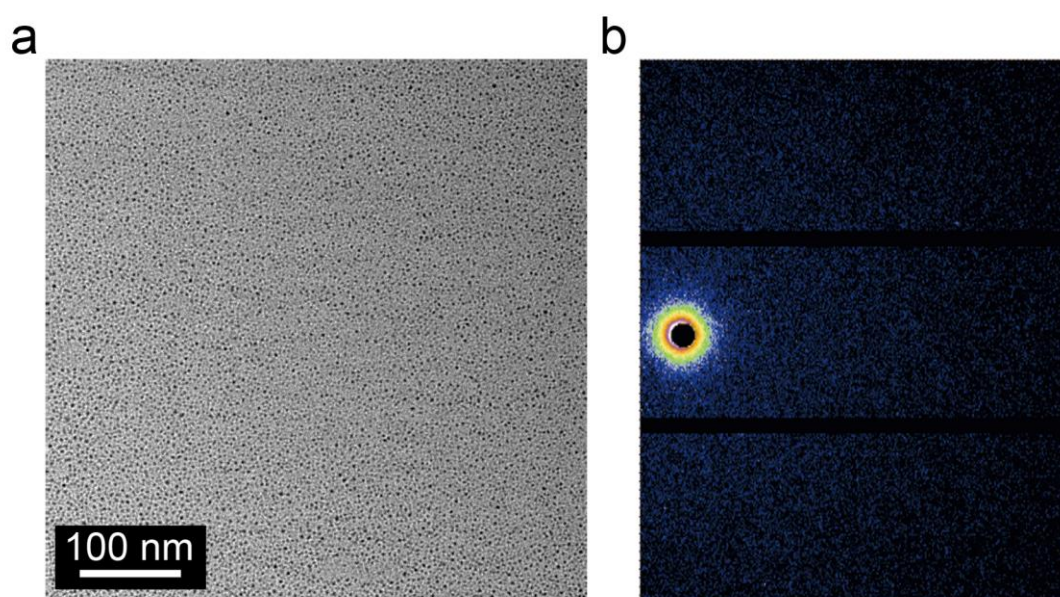


Fig. S17. TEM image of (MoS₂ QSs-PMMA) cross-section (a) and corresponding SAXS image (b).

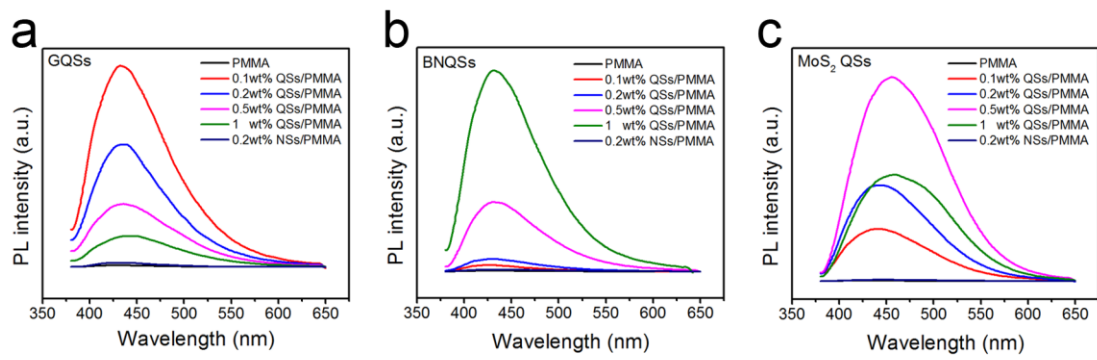


Fig. S18. PL spectra of Qs-PMMA thin films at the excitation wavelength of 360 nm.